Int j simul model 21 (2022) 2, 341-351
Original scientific paper

NUMERICAL ANALYSIS ON MULTIPHASE FLOW IN NEAR-WALL AND NEAR-BOTTOM AREAS

Liu, Z. H.; Wu, J. F.; Hu, T. & Xu, Y. L.[#]
School of Mechanical Engineering, Guiyang University, Guiyang 550005, China
E-Mail: jx0012@gyu.edu.cn ([#] Corresponding author)

Abstract
To mix a solid-liquid multiphase flow more uniformly before filling, this paper numerically analyses the multiphase flow field distribution in the near-wall and near-bottom areas in the agitator tank under the effect of spiral ribbon-frame combined paddle, with the aid of the Eulerian multiphase flow model. The results show that, compared to the spiral ribbon paddle, the combined paddle structure with an additional frame paddle could weaken the high-density aggregation in near-wall and near-bottom areas, and reduce the low-density area on the top, making the flow more uniform. As far as the near-wall area is concerned (200-220 mm from the centre), compared to the combined paddle with oblique outer frame, the combined paddle with straight outer frame improves the uniformity of density distribution for the mixed multiphase flow, stabilizes the volume fraction of each single phase, and reduces the deviation from the set value (4 % - 17 %). The numerical analysis may guide the flow mechanism research of the mixing process of complex solid-liquid multiphase flow, and promote the optimal design of mixing structures.
(Received in February 2022, accepted in May 2022. This paper was with the authors 1 month for 1 revision.)

Key Words: Multiphase Flow, Spiral Ribbon-Frame Combined Paddle, Near-Wall Area, Near-Bottom Area, Flow Mechanism

1. INTRODUCTION

In recent years, the analysis of fluid flow features, especially the numerical calculation of the flow field in near-wall and near-bottom areas, becomes a research hotspot, thanks to the advancement in computer technology, numerical analysis techniques, experimental verification methods, and fluid research strategies [1-3]. Many research results have been achieved in this field.

With the help of Ansys CFX, a fluid mechanics software program, Li et al. [4] preliminarily simulated the agitating power number of the CBY III paddle in the agitator tank under the critical condition of complete off-bottom suspension, and found that the simulated liquid phase velocity and agitating power number in the near-wall area agree well with the experimental values. Through particle image velocimetry (PIV), Lee and Lee [5] studied the near-wall turbulence in the groove structure, revealing that most streamwise vortices reduces drag through the interaction with groove peak, and increases drag through the interaction with groove. By numerical simulation, Zhang et al. [6] explores the generation mechanism of coherent structure in the near-wall area of the turbulence boundary layer, under external disturbance, and effectively improves the theory on a single coherent structure. Through direct numerical simulation, Zhao [7] systematically examined the features of spherical particles in fixed positions in the near-wall area flowing around a body. Using the large wall eddy model, Bermejo-Moreno et al. [8] analysed the correlation between the turbulence boundary layer and the incident shock wave.

Wang et al. [9] experimentally compared the number, mean size, and mean intensity of spanwise vortices at different positions in the near-wall area, and investigated the influence of groove over the spanwise vortices in the near-wall area. In the case of high Reynolds number, Mathis et al. and Marusic et al. [10, 11] studied the amplitude modulation of the large-scale structure and small-scale pulsation in the near-wall area. Wu et al. [12] numerically solved the

formation mechanism and changing features of the symmetric and asymmetric coherence structures in the turbulence boundary layer within the near-wall area. Through global dynamic large eddy simulation and moving mesh simulation, Guo and Zhang [13] probed into the distribution of pressure, velocity, and vorticity, and the turbulence features of the near-wall area in water turbines. By the Eulerian multiphase flow, Du et al. [14] researched the distribution laws of the flow field within horizontal combined agitator tank, including the distribution laws of velocity, density, and single-phase distribution. Xu et al. [15] analysed flow field within the static spiral cutter via computer simulation, focusing on the pressure drop and flow law.

It is easy to see that extensive studies have been conducted on the flow field in near-wall or near-bottom area. However, few scholars have explored multiphase flows with complex components, particularly the solid-liquid mixed seasonings. It is very necessary to numerically analyse the near-wall and near-bottom properties of multiphase flows. Solid-liquid mixed seasonings are common food composed of liquid and complex solid particles. With a poor mixing uniformity, solid-liquid mixed seasonings generally need to be mixed uniformly before filling. The uniformity directly affects the product quality. Therefore, it is very meaningful to explore the mixing properties of such a complex multiphase flow.

Contraposing a solid-liquid mixed seasoning, this paper numerically simulates the distribution of density field and single-phase volume fraction of the multiphase flow in the near-wall and near-bottom areas under the effect of spiral ribbon-frame combined paddle, and further compares the near-wall flow field distributions under the effect of agitators with different structures. The research results provide a reference for understanding the formation of the near-wall and near-bottom flow mechanism for the multiphase flows of solid-liquid mixed seasonings, and for optimizing the agitator structure.

2. BASIC PARAMETERS OF MATERIALS AND AGITATOR STRUCTURE

For simplicity, the target complex solid-liquid mixed seasoning was regarded as a four-phase flow of one liquid phase and four solid phases. Table I lists the specific parameters of the four-phase flow.

Table I: Basic parameters of materials.

	Density (kg/m^3)	**Mean particle diameter** (mm)	**Volume fraction**
Liquid phase	800	--	50 %
Solid phase a	1030	0.5	20 %
Solid phase b	1300	1	20 %
Solid phase c	1860	1	10 %

Considering the large density difference between the single phases in the multiphase flow, this paper chooses the double spiral ribbon paddle with an obvious flow mixing effect in the vertical direction as the main paddle. To enhance the mixing uniformity near the wall and bottom, a frame paddle was added as the auxiliary paddle. The two paddles were combined into the spiral ribbon-frame combined paddle. As shown in Fig. 1, the spiral ribbon-frame combined paddle consists of a groove **a**, a spiral ribbon main paddle **b**, an agitating shaft **c**, and a frame auxiliary paddle **d**. The agitating shaft **c** is connected to two staggered spiral ribbon main paddle, and three evenly distributed frame auxiliary paddles. The frame auxiliary paddle **d** is deployed on the outside of the spiral ribbon main paddle **b**. The relevant parameters are as follows: For the groove **a**, the diameter D = 480 mm, and height H = 400 mm; for the agitating

shaft **c**, the height above the bottom of the groove **a** h_1 = 80 mm; for the spiral ribbon main paddle **b**, the half pitch p = 75 mm; for the frame auxiliary paddle **d**, the height h_2 = 220 mm, the radius is 190 mm, and the width is 30 mm; The fluid depth h_3 = 370 mm.

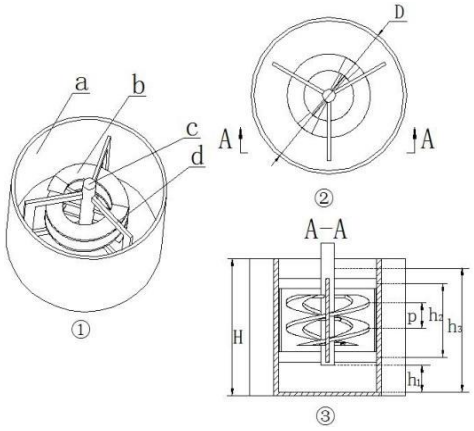

Figure 1: Agitator structure.

3. CALCULATION MODEL

In fluid mechanics calculation, the most common multiphase flow models are volume of fluid (VOF), Mixture model, and Eulerian model. The relatively complex Eulerian model was adopted to illustrate the interaction between single phases of the multiphase flow more accurately. The Eulerian multiphase flow model solves each single phase by multiple continuity equations and momentum equations. The governance equations are as follows:

For the continuity equation, the q^{th} phase is:

$$\frac{\partial}{\partial t}(\alpha_q \rho_q) + \nabla \cdot (\alpha_q \rho_q \vec{v}_q) = \sum_{p=1}^{n} \dot{m}_{pq} \tag{1}$$

For the momentum equilibrium equation, the q^{th} phase is:

$$\frac{\partial}{\partial t}(\alpha_q \rho_q \vec{v}_q) + \nabla \cdot (\alpha_q \rho_q \vec{v}_q \vec{v}_q) = -\alpha_q \nabla p + \nabla \cdot \overline{\overline{\tau_q}} + \sum_{p=1}^{n} (\vec{R}_{pq} + \dot{m}_{pq} \cdot \vec{v}_{pq}) + \alpha_q \rho_q (\vec{F}_q + \vec{F}_{lift,q} + \vec{F}_{Vm,q}) \tag{2}$$

For the pressure strain tensor, the q^{th} phase is:

$$\overline{\overline{\tau_q}} = \alpha_q \mu_q \left(\nabla \cdot \vec{v}_q + \nabla \cdot \vec{v}_q{}^T\right) + \alpha_q \left(\lambda_q - \frac{2}{3}\mu_q\right) \nabla \cdot \vec{v}_q \cdot \bar{\bar{I}} \tag{3}$$

where, $\vec{v}_q$ is the velocity of the q^{th} phase (m/s); $\dot{m}_{pq}$ is the mass transfer from the p^{th} phase to the q^{th} phase (g); p is the shared pressure of all phases (N); $\vec{R}_{pq}$ is the interaction force between the phases (N); $\vec{F}_q$ is the external volume force (N); $\vec{F}_{lift,q}$ is the lift force (N); $\vec{F}_{Vm,q}$ is the virtual mass force (N); μ_q is the shear viscosity of the q^{th} phase (Pa·s); λ_q is the volume viscosity of the q^{th} phase (Pa·s).

4. NUMERICAL CALCULATION

4.1 Grid model

For the liquid-solid-solid-solid four-phase flow, the main body was meshed into tetrahedral grids, which have a small computing load. The special areas, including near-wall, near-paddle,

and near-bottom areas, were meshed into hexahedral grids, which boast high precision and high quality, and refined in local areas. Finally, the multiphase flow was divided into 623,871 grids. Fig. 2 shows the grid model.

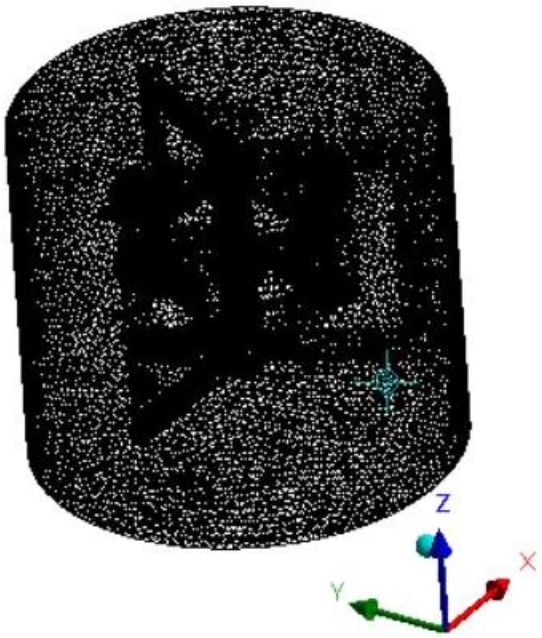

Figure 2: Grid model.

4.2 Solving settings

The multiphase flow in the agitator tank was simulated on FLUENT, with the top liquid surface as the free surface. The wall of the near-wall area was enhanced, and set as a no-slip boundary. The contact surface between the spiral ribbon-frame combined paddle and the multiphase flow was treated as a surface rotating at 5 rad/s.

Conducts the simulation analysis, the top level is free side, Near-Wall Area sets the wall enhancement process, the wall is set to no slip boundary, the screw-frame combination paddle is in contact with Multiphase FLOW. The surface is a rotating surface, and its rotational speed is set to 5 rad/s.

5. RESULTS ANALYSIS

5.1 Density field

To reveal the near-wall and near-bottom flow field distribution of the multiphase flow under the effect of the combined paddle, this section compares the density field distributions of the multiphase flow under the effect of the spiral ribbon paddle, and the spiral ribbon-frame combined paddle, with the aid of the density cloud maps for the vertical surface and horizontal surfaces, and the density curves along the vertical direction and the horizontal direction.

(1) Cloud map of density distribution

Fig. 3 shows the density cloud maps of the multiphase flow under the effect of a single spiral ribbon paddle and the combined paddle on the vertical surface (Y = 0) and horizontal surfaces (Z = 100 mm, 200 mm, 300 mm) of the fluid area. It can be observed that: compared to the spiral ribbon paddle, the combined paddle structure with an additional frame paddle could weaken the high-density aggregation in near-wall and near-bottom areas, and reduce the low-density area on the top, making the flow more uniform.

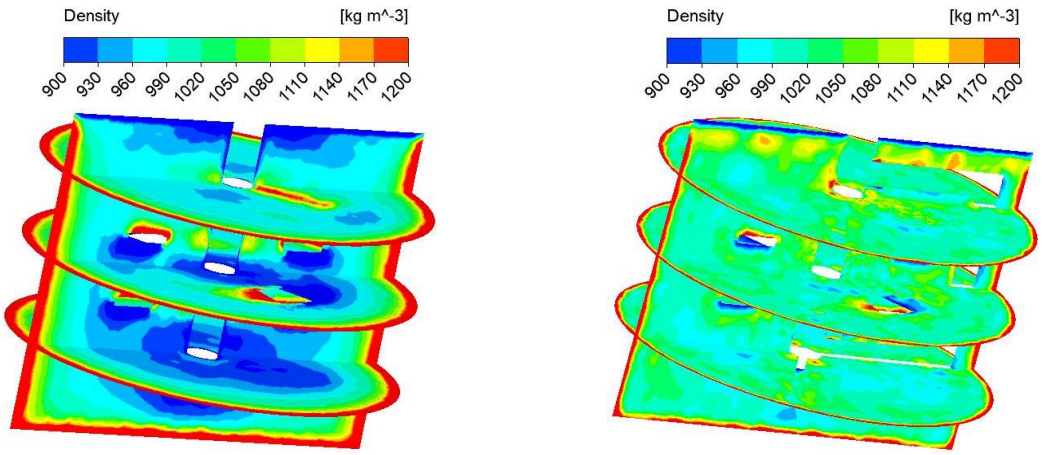

a) Effect of spiral ribbon paddle b) Effect of spiral ribbon-frame combined paddle

Figure 3: Density cloud maps.

(2) Distribution of density curves

1) Near-bottom area

Fig. 4 presents the Z-direction density curves under the effect of a single spiral ribbon paddle and the combined paddle. The four curves are l1 (A1 (50, 0,0) to B1 (50, 0,370)), l2 (A2 (100, 0,0) to B2 (100, 0,370)), l3 (A3 (150, 0,0) to B3 (150, 0,370)), and l4 (A4 (200, 0,0) to B4 (200, 0,370)). It can be learned that: In both agitators, the multiphase flow was relatively dense in the bottom area of the groove. In the near-bottom area (0-25 mm above the bottom), the multiphase flow density in the agitator tank with only the spiral ribbon paddle fell in [1,100, 1,480], while that in the agitator tank with the combined paddle ranged between 1,060 and 1,280. Comparatively, the latter density had a smaller deviation from the mean density of the mixed multiphase flow (1,052 kg/m^3). Therefore, the combined paddle has a better agitating effect than the single spiral ribbon paddle.

2) Near-wall area

Fig. 5 shows the X-direction density curves under the effect of a single spiral ribbon paddle and the combined paddle. The three curves are m1 (C1 (-220, 50,100) to D1 (220, 50,100)), m2 (C2 (-220, 50,200) to D2 (220, 50,200)), and m3 (C3(-220, 50,300) to D3 (220, 50,300)). It can be observed that: the density in the near-wall area (away from the origin) was higher than that in the centre. Under the effect of the spiral ribbon paddle, the multiphase flow density at 200-220 mm from the centre fell in [1,300, 1,550]. After adding the frame paddle, the combined paddle changed the density in the area to [1,150, 1,360], which is closer to the mean density of the fluid (1,052 kg/m^3). Therefore, the frame auxiliary paddle clearly improves the mixing uniformity in the near-wall area.

To further reveal the effects of the frame auxiliary paddle on the distribution of near-wall density field, the authors separately analysed the density distribution under the effect of oblique outer frame paddle and the straight outer frame paddle. Fig. 6 compares the structures of combined paddle with straight outer frame ①, and combined paddle with oblique outer frame ②. Fig. 7 displays the three X-direction density curves (m1, m2, and m3) under the effect of the combined paddle with oblique outer frame. Comparing Fig. 7 with Fig. 5 b (the X-direction density curves under the effect of the combined paddle with straight outer frame), it can be seen that the multiphase flow density belonged to [1,200, 1,380] in the near wall area (200-220 mm from the centre) under the effect of the combined paddle with oblique outer frame. The mixing effect was between that of spiral ribbon paddle, and that of combined paddle with straight outer frame. The reason is that the combined paddle with oblique outer frame has a poor agitating effect than the combined paddle with straight outer frame in the circumferential direction.

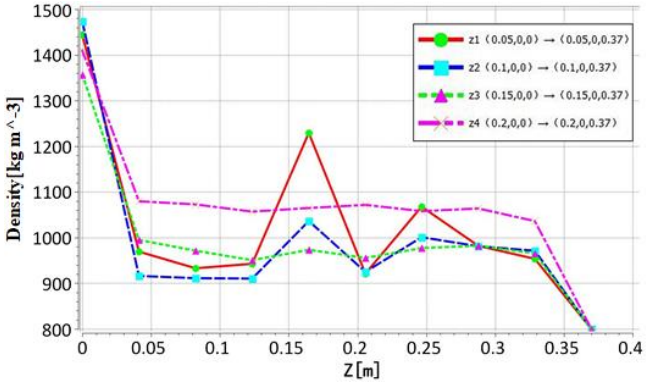

a) Effect of spiral ribbon paddle

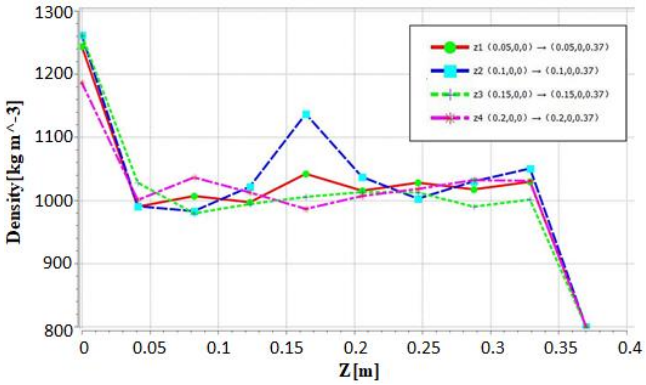

b) Effect of spiral ribbon-frame combined paddle

Figure 4: Z-direction density curves.

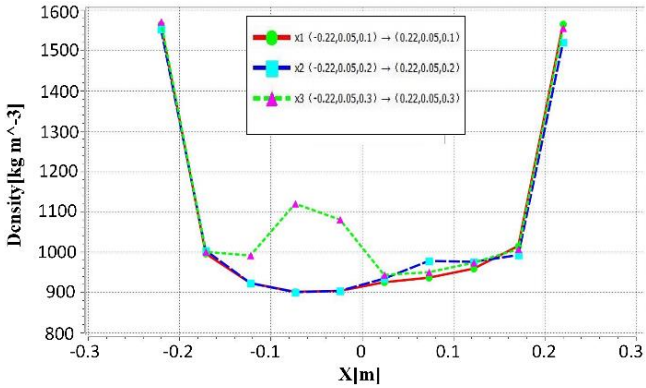

a) Effect of spiral ribbon paddle

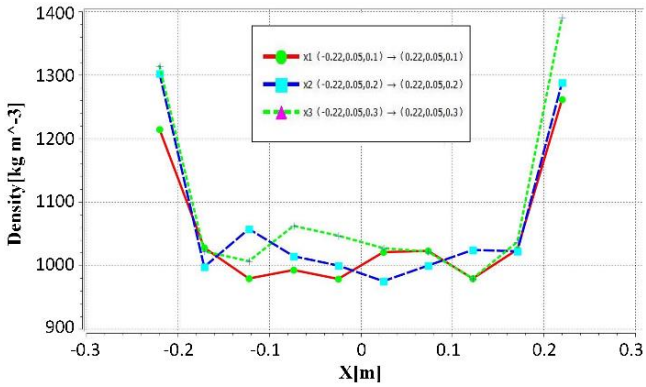

b) Effect of spiral ribbon-frame combined paddle

Figure 5: X-direction density curves.

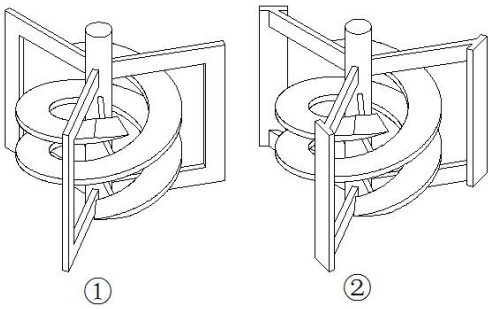

Figure 6: Structures of combined paddle with straight outer frame and combined paddle with oblique outer frame.

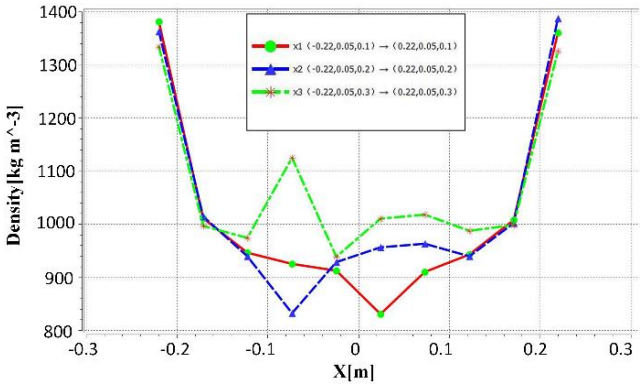

Figure 7: X-direction density curves under the effect of combined paddle with oblique outer frame.

5.2 Volume fraction distribution of each phase

To disclose the agitating effect of combined paddle with straight outer frame and combined paddle with oblique outer frame, the authors went on to analyse the volume fraction distribution of each phase under the effect of each combined paddle. Fig. 8 provides the X-direction density curves (m1, m2, and m3) of each single phase.

The results show that: For the low-density first phase (liquid phase) and second phase (solid phase a), the near-wall volume fractions were smaller than the set values; In the area 200-220 mm from the centre, the volume fraction of the first phase under the effect of combined paddle with straight outer frame was 17 % closer to the set value than that under the effect of combined paddle with oblique outer frame; the volume fraction of the second phase under the effect of combined paddle with straight outer frame was 4 % closer to the set value than that under the effect of combined paddle with oblique outer frame.

For the high-density third phase (solid phase b) and fourth phase (solid phase c), the near-wall volume fractions were above the set values. Under the action of the wall, high-density aggregation was very likely to occur in the near wall area (consistent with the results of density field analysis). In the area 200-220 mm from the centre, the volume fraction of the third phase under the effect of combined paddle with straight outer frame was 5 % closer to the set value than that under the effect of combined paddle with oblique outer frame; the volume fraction of the fourth phase under the effect of combined paddle with straight outer frame was 7 % closer to the set value than that under the effect of combined paddle with oblique outer frame.

In addition, the combined paddle with straight outer frame suppressed the deviation of single-phase volume fraction from the set value in the centre area by different degrees.

Overall, the combined paddle with straight outer frame has a better agitating effect than the combined paddle with oblique outer frame, especially in the near-wall area. Replacing the latter with the former would make the mixing density more uniform, and stabilize the distribution of volume fraction of each single phase.

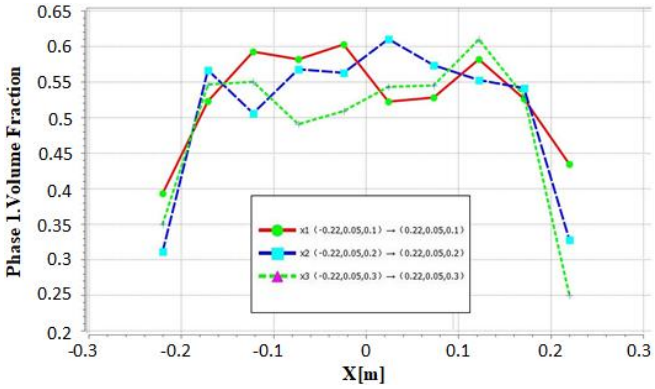

I) combined paddle with straight outer frame

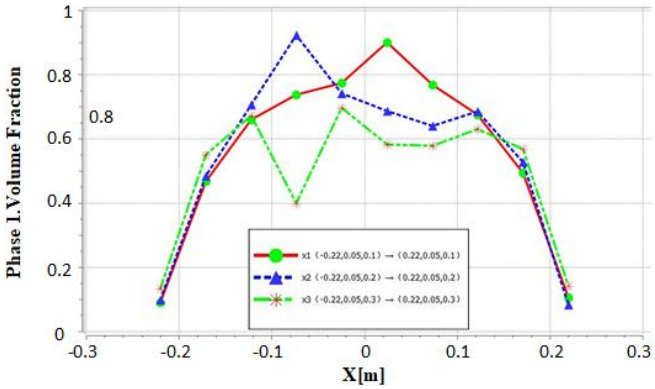

II) combined paddle with oblique outer frame

a) The first phase (liquid phase)

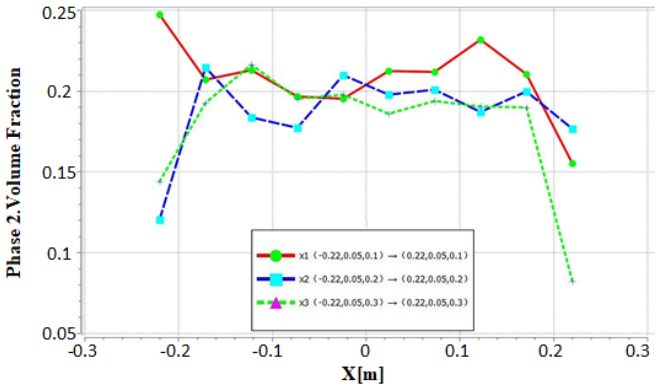

I) combined paddle with straight outer frame

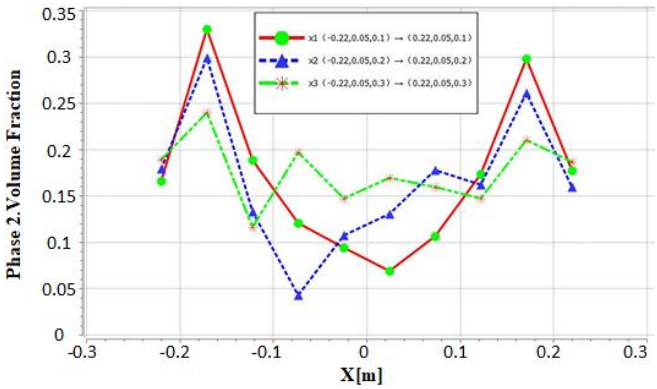

II) combined paddle with oblique outer frame

b) The second phase (solid phase a)

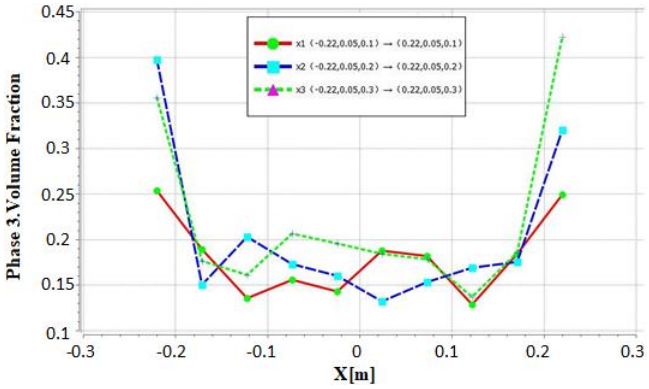

I) combined paddle with straight outer frame

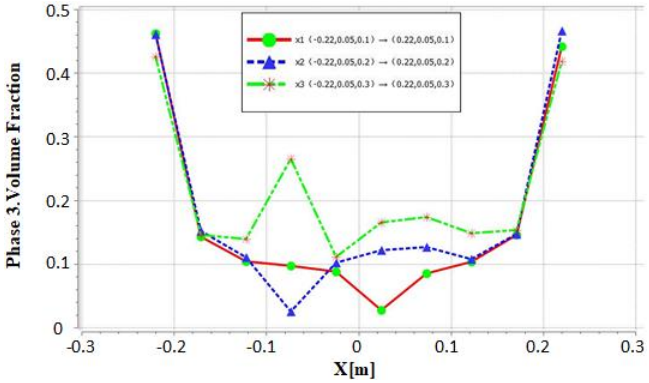

II) combined paddle with oblique outer frame

c) The third phase (solid phase b)

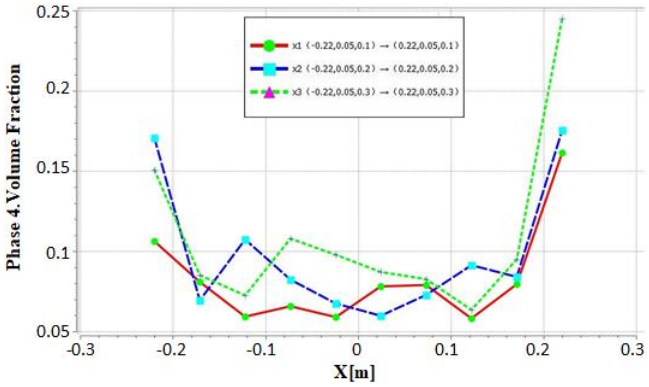

I) combined paddle with straight outer frame

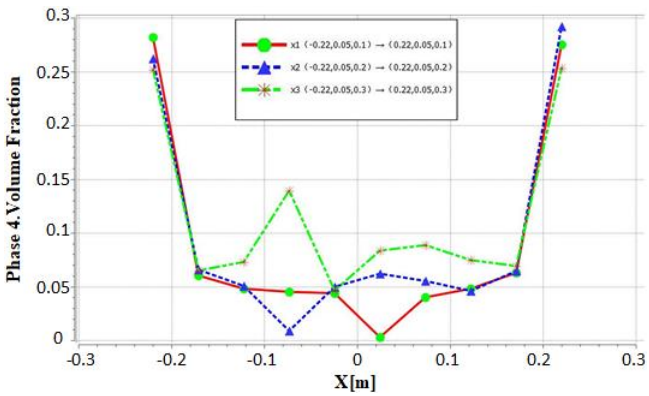

II) combined paddle with oblique outer frame

d) The fourth phase (solid phase c)

Figure 8: Volume fraction distribution curves of each single phase.

6. CONCLUSIONS

Using FLUENT, this paper numerically solves the density field of a multiphase flow, and the volume fraction distribution of each single phase, under the effect of combined paddle with straight outer frame, spiral ribbon paddle, and combined paddle with oblique outer frame. The research provides insights into the flow field distribution in the near-wall and near-bottom areas in the agitator tank. The main conclusions are as follows:

(1) Compared to the spiral ribbon paddle, the combined paddle structure with an additional frame paddle could weaken the high-density aggregation in near-wall and near-bottom areas, and reduce the low-density area on the top, making the flow more uniform.

(2) As far as the near-wall area is concerned (200-220 mm from the centre), the combined paddle with oblique outer frame has a mixing effect between that of spiral ribbon paddle, and that of combined paddle with straight outer frame.

(3) The volume fraction of each single phase in the multiphase flow deviates from the set value smaller under the effect of combined paddle with straight outer frame than under the effect of combined paddle with oblique outer frame. This is particularly true in the near-wall area (200-220 mm from the centre), where replacing combined paddle with oblique outer frame with combined paddle with straight outer frame can reduce the deviation of the volume fraction distribution of each single phase by around 10 %, and significantly enhance the mixing uniformity.

ACKNOWLEDGEMENTS

This work was financially supported by the National Natural Science Foundation of China (Grant No.: 52105248), the science and technology top talent project of Guizhou Provincial Department of Education, the special funding of Guiyang science and technology bureau and Guiyang University (GYU-KY-[2021]), the Natural Science Foundation of Guizhou Province ([2020]1Y226).

REFERENCES

[1] Yin, M.; Xu, L. J.; Dai, Y.; Yang, D.; Zhu, X. (2021). Flow characteristics of oil-guiding splash lubrication: simulation and experiment studies, *International Journal of Simulation Modelling*, Vol. 20, No. 2, 363-374, doi:10.2507/IJSIMM20-2-CO6

[2] Deb, H. R. (2021). Hydromagnetic second-order fluid flow in a channel with fluid-particle suspension and viscous dissipation, *International Journal of Heat and Technology*, Vol. 39, No. 5, 1673-1679, doi:10.18280/ijht.390532

[3] Rajakumar, K. V. B.; Rayaprolu, V. S. R. P. K.; Balamurugan, K. S.; Kumar, V. B. (2020). Unsteady MHD Casson dissipative fluid flow past a semi-infinite vertical porous plate with radiation absorption and chemical reaction in presence of heat generation, *Mathematical Modelling of Engineering Problems*, Vol. 7, No. 1, 160-172, doi:10.18280/mmep.070120

[4] Li, L. C.; Zhang, Z. M.; Huang, X. B. (2005). Study on the liquid phase velocity near wall in a solid-liquid stirred tank, *Journal of Beijing University of Chemical Technology (Natural Science Edition)*, Vol. 32, No. 1, 33-38, doi:10.3969/j.issn.1671-4628.2005.01.008

[5] Lee, S.-J.; Lee, S.-H. (2001). Flow field analysis of a turbulent boundary layer over a riblet surface, *Experiments in Fluids*, Vol. 30, No. 2, 153-166, doi:10.1007/s003480000150

[6] Zhang, D. M.; Luo, J. S.; Zhou, H. (2005). A mechanism of excitation of coherent structures near the wall by disturbances in the outer region of the turbulent boundary layer, *Applied Mathematics and Mechanics*, Vol. 26, No. 4, 379-385, doi:10.3321/j.issn:1000-0887.2005.04.001

[7] Zhao, H. (2016). *Direct Numerical Simulation of Flow Characteristics Around a Particle in Proximity to a Wall*, Zhejiang University, Hangzhou (in Chinese)

[8] Bermejo-Moreno, I.; Campo, L.; Larsson, J.; Bodart, J.; Helmer, D.; Eaton, J. K. (2014). Confinement effects in shock wave/turbulent boundary layer interactions through wall-modelled large-eddy simulations, *Journal of Fluid Mechanics*, Vol. 758, 5-62, doi:10.1017/jfm.2014.505

[9] Wang, X.; Li, S.; Tang, Z. Q.; Jiang, N. (2018). An experimental study on riblet-induced spanwise vortices in turbulent boundary layers, *Journal of Experiments in Fluid Mechanics*, Vol. 32, No. 1, 55-63, doi:10.11729/syltlx20170092

[10] Mathis, R.; Hutchins, N.; Marusic, I. (2009). Large-scale amplitude modulation of the small-scale structures in turbulent boundary layers, *Journal of Fluid Mechanics*, Vol. 628, 311-337, doi:10.1017/S0022112009006946

[11] Marusic, I.; Mathis, R.; Hutchins, N. (2010). Predictive model for wall-bounded turbulent flow, *Science*, Vol. 329, No. 5988, 193-196, doi:10.1126/science.1188765

[12] Wu, W. G.; Lu, C. G.; Xue, S. F. (2013). Formation mechanism of symmetric and asymmetric coherent structures in near wall turbulent boundary layer, *Acta Aerodynamica Sinica*, Vol. 31, No. 4, 420-424

[13] Guo, T.; Zhang, L. X. (2014). Study on near wall turbulence characteristics and flow field structure of draft tube of Francis turbine, *Transactions of the Chinese Society for Agricultural Machinery*, Vol. 45, No. 9, 112-118, doi:10.6041/j.issn.1000-1298.2014.09.019

[14] Du, F. L.; Li, S. B.; He, L. (2013). Simulation analysis of solid-liquid mixture multiphase flow in horizontal combined stirred tank, *Food & Machinery*, Vol. 29, No. 5, 111-114

[15] Xu, Z. W.; Cui, Z. W.; Yuan, F. Y.; Wu, C. (2018). Computational fluid dynamic simulation flow field and pressure drop characteristics of the gas-liquid two phase flow in a static spiral cutter, *Food & Machinery*, Vol. 34, No. 3, 89-92+165, doi:10.13652/j.issn.1003-5788.2018.03.019